Separation and Purification Technology 354 (2025) 128769

Contents lists available at ScienceDirect

Separation and Purification Technology

journal homepage: www.elsevier.com/locate/seppur

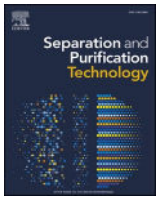

Streamlining the purification of a clinical-grade oncolytic virus for therapeutic applications

Rita P. Fernandes [a,b,1], Sven Göbel [c,1], Manfred Reiter [d], Alexander Bryan [e], Jennifer Altomonte [e], Yvonne Genzel [c], Cristina Peixoto [a,b,*]

[a] iBET, Instituto de Biologia Experimental e Tecnológica, Apartado 12, 2780-901 Oeiras, Portugal
[b] Instituto de Tecnologia Química e Biológica António Xavier, Universidade Nova de Lisboa, Avenida da República, 2780-157 Oeiras, Portugal
[c] Bioprocess Engineering, Max Planck Institute for Dynamics of Complex Technical Systems, Magdeburg, Germany
[d] Nuvonis Technologies GmbH, Vienna, Austria
[e] Department of Internal Medicine II, Klinikum Rechts der Isar, Technische Universität München, Munich, Germany

ARTICLE INFO

Editor: Raquel Aires Barros

Keywords:
Oncolytic virus
Downstream processing
Anion-exchange chromatography
Cancer treatment
Manufacturing

ABSTRACT

Oncolytic viruses (OV) have emerged as a promising approach to mitigate the challenges of treating solid cancers. However, the lack of established manufacturing and downstream processing (DSP) platforms combined with the high treatment doses needed for clinical use (10^8–10^{11} $TCID_{50}$/dose), hamper the widespread success of this therapeutic concept. Here, we present an efficient and scalable GMP-compliant process for the purification of a fusogenic oncolytic virus (rVSV-NDV). Non-GMO CCX.E10 cells grown in suspension in chemically defined medium were used for high titer rVSV-NDV batch production (3.2×10^8 $TCID_{50}$/mL) in stirred tank bioreactors. All DSP unit operations (DNA digestion, clarification, chromatography, TFF, and sterilizing filtration) were optimized to identify the best purification approach. Among several strategies evaluated, two filters enabled high throughput and turbidity reduction, while preventing any loss of infectious particles during the clarification step. For the intermediate purification, anion-exchange chromatography (AEX) was used in combination with the addition of polyprotic salts, which resulted in a maximum recovery yield of 86 % of infectious particles. The addition of citrate to the chromatography setup increased the separation resolution of rVSV-NDV particles from less negatively charged impurities. Global recovery yield after four operation units was 64 % with 99 % and 97 % of protein and DNA clearance, respectively. Together, with our previously optimized upstream process, we open up an avenue for large-scale manufacturing of oncolytic VSV-NDV for future clinical use.

1. Introduction

Traditional chemotherapy drugs and radiation therapy often have limited success in treating late-stage cancers due to their non-specific targeting and resistance mechanisms of the tumor [1]. Furthermore, due to the immune-suppressive tumor microenvironment that is characteristic of many solid tumors, immunotherapies such as CAR-T cells or immune checkpoint inhibitors are only minimally effective in these cancers [2]. As a promising alternative, virus-based biotherapeutic particles, known as oncolytic viruses (OVs), which can selectively infect and kill cancerous cells, are gaining attention [2]. T-VEC (Amgen), an oncolytic HSV-1 expressing GM-CSF, was the first and is currently still the only FDA-approved oncolytic viral immunotherapy for the treatment of metastatic melanoma [3]. Characterized by their pleiotropic mode of action, OVs can cause direct lysis of tumor cells without harming surrounding healthy tissue with a secondary therapeutic initiation of systemic antitumor immunity [4]. To improve their efficacy, many OVs are additionally modified through genetic engineering, for example to express optimized endogenous or heterologous fusion glycoproteins, ideally serving as platforms for the insertion of various therapeutic genes. An engineered hybrid vector comprising components of vesicular stomatitis virus (VSV) and Newcastle disease virus (NDV) has previously been shown to be safe and efficient for the treatment of hepatocellular carcinoma in pre-clinical tumor models [5]. In light of this promising preclinical data, there is an urgent need for efficient and scalable manufacturing processes, which can cope with the complexity of such

* Corresponding author at: iBET, Instituto de Biologia Experimental e Tecnológica, Oeiras, Portugal.
E-mail address: peixoto@ibet.pt (C. Peixoto).
[1] These authors contributed equally.

https://doi.org/10.1016/j.seppur.2024.128769
Received 3 June 2024; Received in revised form 9 July 2024; Accepted 9 July 2024
Available online 10 July 2024

products [6].

Several OVs have been developed and used in clinical applications to date; however, the diversity of these biotherapeutic particles poses major challenges for downstream processing (DSP) and necessitates the development of individualized processes that are optimized for each virus, thereby posing an additional challenge to clinical translation [1,7]. These challenges are amplified by the need for highly concentrated doses to achieve the desired oncolytic effect, as compared to vaccines for which the input requirement is significantly lower [1]. Additionally, these OVs pose structural challenges to the process development, owing to their large size (>150 nm), but also due to their morphology and complexity of surface charges [8]. As the virus size can be greater than the pore size of resin beads in the chromatographic column, the dynamic binding capacities (DBC) in chromatographic strategies can be impaired. Also, the shear stress during filtration-based steps can be detrimental to the integrity of the virus particles [8,9]. OV platforms based on enveloped viruses like rVSV-NDV, herpesvirus, vaccinia virus, and measles virus present further challenges for DSP purification due to their sensitivity to physiochemical stress. Nevertheless, most OV platforms currently investigated in clinical trials or approved on the market, share common steps and unit operations [1,10]. Previous studies have shown promising purification approaches using single-mode chromatography such as anion- or cation- exchange (AEX, CEX) and affinity [11–13].

As OVs are categorized as gene therapy medical products by the European Medicine Agency (EMA), production and final downstream processing (DSP) must comply with specific guidelines [14,15]. To achieve a therapeutic effect and effective delivery to tumor sites, final dose inputs of rVSV-NDV in the range of 10^9-10^{11} virions/injection are required, imposing high virus concentration to achieve small-volume doses with the quality desirable. Host cell protein (HCP) and host cell DNA (hcDNA) should not exceed 100 ng/mL and 10 ng per dose, respectively [16]. Lastly, the ratio of noninfectious to infectious particles, while not exactly defined, should be minimal for the final product, and high oncolytic potency in the target cell must be maintained. These quality attributes require a delicate interplay between upstream and downstream process development steps to maintain virus activity and yield, while removing an adequate level of impurities.

Particularly for fusogenic OVs, such as rVSV-NDV, usage of adherent cell culture systems only results in very low virus titers (~10^6 $TCID_{50}$/mL) due to the rapid formation of large multinucleated syncytia, before sufficient titers can be reached [5]. Ideally, manufacturing should shift towards fully characterized, continuous suspension cell culture using chemically defined media to allow for easy scale-up and usage of advanced process monitoring controls. Recently, a fully characterized, non-GMO continuous suspension cell line derived from a quail (CCX.E10) was reported to produce rVSV-NDV titers up to 4.2×10^8 $TCID_{50}$/mL in batch mode [17]. In this work, subsequent DSP challenges following such a production of rVSV-NDV in CCX.E10 cells are addressed. Here we report for the first time, a purification strategy of a fusogenic OV using AEX chromatography, followed by tangential flow filtration (TFF) and sterilizing filtration. Process development was performed with the objective of a full GMP-compliant manufacturing process. We were able to achieve a recovery of 64 % infectious virus with a titer of 4×10^9 $TCID_{50}$/mL, which is well within the range of industry standards for commercial virus production.

2. Material and methods

2.1. Cell lines and virus production

CCX.E10 cells (Nuvonis Technologies GmbH) were cultured in suspension in chemically defined Freestyle™293 Expression medium (Gibco, USA) supplemented with growth factors. Cells were maintained at 37 °C and 5 % CO_2 in a multitron orbitally shaker incubator (Infors AG, Switzerland) with a 50 mm shaking diameter in baffled 125 mL shake flasks (Corning, USA) and passaged twice per week. Adherent Huh7 cells and AGE1.CR.pIX were cultured in T75 flasks using either high glucose Dulbecco's Modified Eagle Medium (DMEM, Gibco, USA) supplemented with 1 mM sodium pyruvate (Gibco, USA), 1 × non-essential amino acids (Gibco, USA), and 10 % fetal calf serum or DMEM-F12 medium (Gibco, USA) supplemented with 5 % fetal calf serum. Both cell lines were incubated at 37 °C with 5 % CO_2.

Viable cell concentration (VCC) and viability were determined with an automated cell counter (ViCell, Coulter Beckman, USA) by trypan blue exclusion. Infections were carried out using a sucrose gradient-purified CCX.E10 cell-derived rVSV-NDV virus seed with a titer of 1.05×10^8 $TCID_{50}$/mL.

Material for initial clarification screening studies as well as DNA digestion studies was produced in 250 mL baffled shake flasks. Here, CCX.E10 cells were inoculated at 0.8×10^6 cells/mL and cultivated until a VCC of 4×10^6 cells/mL was reached. At time of infection (TOI), cells were diluted two-fold with fresh medium, infected at an MOI of 1E-4, and harvested once cell viability fell below 90 % (48–60 hpi). After harvest, material was either centrifuged at 3000*g* for 10 min at 4 °C, supplemented with 5 % sucrose and frozen at −80 °C (frozen material), or supplemented with 5 % sucrose and directly subjected to further processing (fresh material). Before usage of frozen material, aliquots were thawed overnight at 4 °C.

All other material was produced as previously described in 1 L or 3 L STR (DasGip, Eppendorf AG, Germany) in batch mode [17]. Briefly, after reaching a VCC of 4.0×10^6 cells/mL, cells were infected at an MOI of 1E-4 by adding an equal working volume (wv) of pre-warmed fresh medium containing rVSV-NDV. pH was maintained at 7.2 by sparging CO_2. Partial pressure of dissolved oxygen (DO) was maintained at 50 % by controlling oxygen and nitrogen flow rates between 3–12 L/h through an L-drilled hole sparger. Cells were agitated using one (1 L STR) or two (3 L STR) pitched blade impellers at 130–180 rpm. All cultures were harvested once cell viability fell below 90 %.

2.2. Nuclease treatment and optimization of DNA digestion

20 U/mL endonuclease (DENARASE®, enzyme activity > 250 U/µl determined by the manufacturer, 20804–500 k; c-Lecta) was mixed with 2 mM MgCl2 to digest DNA in the supernatant. The digestion was carried out at room temperature for 1 h

For optimization, a central composite faced (CCF) design of experiments (DoE)-design was chosen to evaluate the DNA digestion. The design factors included the endonuclease activity (20, 60, 100 U/mL), incubation time (1, 3.5, 6 h), and incubation temperature (20, 28.5, 37 °C). For this purpose, 1 mL aliquots of virus-containing cell broth harvested at 60 hpi was supplemented with 5 % sucrose and prepared in 1.5 mL reaction tubes. Immediately afterward, 2 mM $MgCl_2$ and the respective endonuclease activity (20,60,100 U/mL) were added. The 2 mM $MgCl_2$ salt solution was prepared in PBS. As a negative control, virus-containing cell culture broth with 5 % sucrose was used. The aliquots were agitated with 600 rpm (2 mm shaking diameter) at the respective temperatures for 1, 3.5, and 6 h. Experiments for each condition were carried out as single runs, except for the center point, which was repeated five times. The readouts were total DNA concentration (picogreen assay), infectious virus titer ($TCID_{50}$ assay), and total protein concentration (BCA assay). The experimental data were analyzed using the software package MODDE® version 13.0 (Sartorius, Germany).

2.3. Clarification

Several dead-end clarification filters with different pore sizes and membrane materials were evaluated for fresh and frozen CCX.E10-derived harvests (Table 1). Prior to clarification, a DNA digestion step was carried out using endonuclease at 20 U/mL for 1 h at room temperature. All depth filters (1.1–1.3; 2.1–2.2) were washed with 230 mL of milli-Q water according to the manufacturer's recommendation.

Table 1
Clarification devices used in the screening experiments.

	Device	Reference	Target step	Chemistry	Screening surface area (cm^2)	Nominal pore size (μm)
1.1	Millistack C0HC	MC0HCC23L3	Primary clarification	Cellulose + filter aid	23	1.2–0.2
1.2	Millistack D0HC	MD0HCC23L3		Cellulose + filter aid	23	10–0.55
1.3	Millistack media CE50	MCE5023CL3		Cellulose	23	1–0.4
2.1	Sartopure PP3	5051306P5-OO	Secondary clarification	Polypropylene	240	0.45
2.2	Sartoguard NF	5461307G4–OO–B		Polyether sulfone	190	0.22

Filters 1.1–1.3 were operated at constant flux of 9 mL/min, while filters 2.1 and 2.2 were operated at constant flux of 27 mL/min. A portable turbidimeter (HACH 2100Q is) was used to measure turbidity before and after clarification.

2.4. Screening of chromatography devices

Virus purification by chromatography was performed in an Äkta Avant 150 equipment (Cytiva), using the software, Unicorn version 6.3, and operated at room temperature. An initial screening of chromatographic devices was carried out with Capto DEAE resin (Cytiva), Sartobind Q membrane (Sartorius Stedim), and Mustang Q (Cytiva) as present in Table 2. All membranes were conditioned following the respective manufacturer's instructions. For Capto DEAE screening, approximately 5 mL of resin was packed in a XK16 column (Cytiva) according to the instructions, and asymmetry factors between 0.8 and 1.5 were obtained. Devices were equilibrated with 5 membrane/column volumes (MV/CV) with equilibration buffer (20 mM Tris, 150 mM NaCl, 5 % sucrose, pH 8.0) before sample loading, and for the scouting experiments the sample loading ranged from 17 MV/CV to 55 MV/CV. The elution buffer composition was 20 mM Tris, 2 M NaCl, 5 % sucrose, pH 8.0. For all experiments, clarified virus material was thawed at 4 °C overnight and equilibrated to room temperature before each experiment.

2.5. Chromatography – Screening of different inorganic salts

The influence of the addition of different inorganic salts (citrate, phosphate, and carbonate) was assessed in the chromatography performance. A 1 M stock solution of each salt was prepared at pH 8.0, and then added individually to the previously mentioned equilibration and elution buffers to a final concentration of 100 mM. A 1 mL Sartobind Q membrane was used for this scouting. The same chromatography parameters were used as in the previous screening.

2.6. Tangential flow filtration

The eluted rVSV-NDV fraction from Sartobind Q was diluted 4-fold (65 mL) and diafiltered 6 times. Subsequently, the virus fraction was concentrated 4-fold using a 750 kDa cut-off hollow fiber polyethersulfone membrane (UFP-750-C-2U) with 50 cm^2. Fibers were first washed with milli-Q water and equilibrated with diafiltration buffer (10 mM Tris, 5 % sucrose, pH 8.0) following the manufacturer's instructions. The input flow rate was 25 mL/min in order to keep the shear rate at 2500 s^{-1}. The purified rVSV-NDV solution was then sterile filtered.

Table 2
Specifications for the different anion exchange chromatography (AEX) media.

Device	Type of adsorber	Ligand	Nominal pore size (μm)
Capto DEAE	Resin	Diethylethanolamine	0.06
Sartobind Q	Membrane	Quarternary ammonium	3
Mustang Q	Membrane		0.8

2.7. Sterile filtration

Sterilizing grade filtration of purified rVSV-NDV was performed with different syringe filters in order to select the best potential candidate. The evaluated filters were Supor® EKV Mini Kleenpak™ (Pall Corporation), MiniSart® (Sartorius Stedim), and Millex-GV (Merck). Before use, the filters were washed with Milli-Q water and equilibrated with diafiltration buffer (20 mM Tris, 5 % sucrose, pH 8.0).

2.8. rVSV-NDV viral genomes quantification

For routine quantification, 100 μL of each sample was treated with DNAse I (Roche) and then RNA extraction was performed using the QIAamp Viral RNA Mini kit (Qiagen). Next, 5 μL of the extracted RNA was used with High Capacity cDNA Reverse Transcription Kit (Applied Biosystems, ThermoFisher Scientific) to generate cDNA using optimized RT-PCR primers. Then, the cDNA was diluted (between 1:1000 to 1:100,000) to target the linear range of ddPCR. 5 μL of the template dilution was used with the QX200 ddPCR kit (Bio-Rad Laboratories, Hercules, CA, USA), using the EvaGreen master mix and the selected primers already described elsewhere[18]. The manufacturer's instructions were followed to prepare the reaction and generate droplets. As for the thermocycler program: after initial denaturation (5 min at 95 °C), 34 cycles of the following steps were repeated: 30 s at 95 °C, 1 min at 59 °C, 30 s at 72 °C. The final elongation step was performed for 5 min at 72 °C.

Droplets were analyzed individually in the droplet reader and the copies/μL of each sample are given. This output is corrected for the dilution and volumes used to determine the viral genomes/mL of the original sample with the following calculation:

$$\frac{Viralgenomes}{mL} = I \times J \times K \times \left(\frac{L}{M}\right) \times \frac{\frac{O}{N}}{P} \times Q \times 1000$$

in which: I = Copies/μL (ddPCR output); J = volume of the ddPCR reaction; K = dilution of the cDNA template; L = volume of RT-PCR reaction; M = volume of the cDNA dilution added in the ddPCR reaction; N = volume of RNA added in the RT-PCR reaction; O = elution volume for RNA extraction; P = initial sample volume used for the RNA extraction; Q = dilution of the sample in RNA extraction

2.9. rVSV-NDV infectious viral particles quantification

Infectious titers of rVSV-NDV were measured as described previously [19]. Briefly, adherent AGE1.CR.pIX cells were seeded in 96-well tissue culture plates to achieve 100 % confluency on the day of infection. Ten-fold serial dilutions of samples were performed to achieve desirable dilution for expected titer range. Six dilutions were added to the plates to inoculate the cell monolayer. After an incubation period of 72 h, plates were analyzed using a light microscope. rVSV-NDV infectious titer was reported in 50 % tissue culture infectious dose ($TCID_{50}$/mL). The variability of the assay was ± 0.2 $\log_{10}$ $TCID_{50}$/mL.

2.10. Defective interfering particles (DIP) genome quantification and analysis

Fixed volumes of 40 μl, derived from chromatography elution

fractions were mixed with 5 µl of 10x DNase digestion buffer, and 5ul of DNase I (reconstituted; 1 U/ul) (Zymo Research). DNase digestion was carried out at room temperature for 15 min in solution. Before RNA extraction, DNase was inactivated at 75 °C for 5 min in 5 mM EDTA. Following DNase inactivation, samples were diluted to total volume of 140 µl in nuclease-free water and immediately mixed with 560 µl of AVL buffer of the QIAamp Viral RNA mini kit (Qiagen, Hilden, Germany). RNA extraction was performed per the manufacturer's protocols with final elution in 40 µl of buffer AVE.

5′ to 3′ trailer inversion events have been reported for VSV defective interfering particle genomes. To specifically amplify RNA sequences containing these inversion regions, a single primer (AAAAAA-TAAAAACCACAAGAGGGTCTTAAG) RT-PCR strategy was applied based on previously reported protocols for VSV [20], with this single primer acting as both a forward and reverse primer during PCR amplification. Reverse transcription reactions of 20 µl were carried out using the high-capacity cDNA reverse transcription kit (Thermo Fisher Scientific), with fixed 10 µl volumes of extracted viral RNA. Prior to mixing with the RT master mix, RNA samples were mixed with 1 µM of target-specific primer, with these mixtures pre-denatured together for 65 °C for 3 min followed by incubation on ice for 2 min. Following reverse transcription, total cDNA was used for PCR amplification. PCR amplification was carried out using ALLin HiFi DNA polymerase kit protocols (highQu, Kraichtal), as per manufacturers' protocols with a 60°c annealing temperature and an extension time of 2.5 min. Final DNA products were assessed on 1 % agarose gels.

2.11. Assessment of product quality

For additional characterization, several analytical techniques were used to evaluate the integrity, purity and identity of the rVSV-NDV.

The size and concentration of rVSV-NDV samples were determined using nanoparticle tracking analysis in the chromatographic DBC studies. Chromatography flow-through samples were diluted (1:10–1:100) in sterile phosphate-buffered saline (PBS) and analyzed (1000 µL) with a Nanosight NS300, by measuring 3 capture replicates of 60 s (Malvern Panalytical, Westborough, MA, USA).

Purified rVSV-NDV samples were analyzed by transmission electron microscopy (TEM). rVSV-NDV virions were fixed in 4 % paraformaldehyde (1:1) at room temperature (2 min), placed (2 µL) on carbon-formvar-coated copper grids (300 mesh), and blotted. Water (2 µL) was added to the samples that were then blotted, and 2 % aqueous uranyl acetate (2 µL) was placed on the grid (2 min) and blotted. The grids were examined with a 208S Electron Microscope (FEI; 60 kV, Philips, Amsterdam, NY, USA). Digital images were obtained with an 831 Orius Camera (Gatan, Pleasanton, CA, USA) and were processed with Adobe Photoshop CS5 (64 bit) software.

The sample labelling procedure for CE-SDS LIF analysis was based on the protocol described by SCIEX (Framingham, MA, USA) [21]. For the purity evaluation analysis, the exact protocol was followed as described by Fernandes et al. [22].

Total protein was assessed with Pierce™ BCA assay kit (ThermoFisher) and total DNA was quantified with Quant-iT™ PicoGreen dsDNA assay kit (ThermoFisher) used according to the manufacturer's instructions.

Oncolytic viral potency was determined using the previously described half maximal inhibitory concentration (IC50) potency assay in Huh7 cells [19].

3. Results

3.1. Screening of primary and secondary clarification filter units

DNA digestion parameters that were previously optimized for clarified rVSV-NDV supernatants produced in HEK293 cells were directly adopted for the DNA digestion step of fresh and frozen CCX.E10 derived material. Here, an enzyme activity of 20 U/mL and an incubation time of 1 h allowed a reduction of 98 % of initial DNA, and these conditions were used for all subsequent DNA digestions steps (Supplement 1).

To select a primary clarification filter, DNA-digested cell broth containing rVSV-NDV, harvested 48 hpi at a culture viability of 81.2 % from shake flasks cultures was used. The scouting revealed that filter 1.3 enabled a complete recovery of infectious virus particles, however, the final solution turbidity remained at 125 NTU, corresponding to a 64 % reduction (Table 3). While filters 1.1 and 1.2 achieved a turbidity reduction greater than 90 %, the recovery of infectious virus particles was poor, lower than 50 %.

As the turbidity reduction for filter 1.3 was inferior to the other filter devices, a second filtration step comprised of filter 2.1 (PP3 0.45 µm) and filter 2.2 (NF 0.22 µm) was tested with frozen material (Table 3). Here, filter 1.3 again allowed a complete recovery of infectious virus particles (IVP) while reducing the solution turbidity by 44.2 % to an amount of 46.2 NTU. Subsequent filtration using filter 2.1 also allowed a complete recovery of IVPs and a further turbidity reduction of 80.7 % to 16 NTU. Using filter 2.2 resulted in a final yield of 42 % with turbidity values below 10 NTU. Therefore, filters 1.3 and 2.1 were selected for clarification of bioreactor crude harvests.

3.2. Investigation of different clarification trains

Optimal clarification trains should remove cells, cell debris, and particulate impurities, resulting in material with substantially reduced turbidity, yet high product recovery. The STRs (1 L and 3 L) were both harvested at 67 hpi when culture viability dropped below 90 %. In a first step, DNA in the crude harvest was digested using the previously described HEK293-based endonuclease digestion step (Supplement 1) and subsequently filtered using two different industry-relevant clarification trains: a combination of filter 1.3 and 2.1 (train 1) or sedimentation at room temperature for 24 h followed by filtration with filter 2.1 (train 2). Crude harvests for both clarification trains were similar in terms of infectious virus titer, solution turbidity, DNA, and protein concentration, as well as cell concentration and cell viability, although produced at different scales (Figure S1).

Both clarification trains achieved a complete recovery of IVPs, while efficiently reducing the solution turbidity by 87 % and 92 %, respectively (Table 4). The endonuclease digestion step of train 1 resulted in a DNA reduction of 78 %. After filtration with filter 1.3 and 2.1, DNA was removed up to 90.5 %. Primary clarification by sedimentation for train 2 did not impact the infectious virus titer and was able to reduce the solution turbidity by 82 % compared to 53.7 % by filtration with filter 1.3. Host cell DNA was reduced by 80 % using the endonuclease digestions step and by 89.2 % after filtration with filter 2.1.

3.3. Optimization of DNA digestion

Direct transfer of the endonuclease digestion step, which was previously optimized for cell-free supernatant of HEK293 cells (Supplement 1), resulted in low DNA digestion efficiencies of 78–80 %. To investigate the effect of the host cell line and the presence of residual cells on the DNA digestion, a DoE was carried out using CCX.E10-derived cell broth. Here, a CCF design with three factors (temperature, incubation time, and endonuclease concentration) was selected for optimization. As expected, total protein concentration remained stable throughout all evaluated conditions and was not affected by the DNA digestion step (data not shown). The two other responses (infectious virus titer and DNA reduction) were fitted to a quadratic polynomial model and evaluated using MODDE®. Here, model fit values (R^2) above 0.94 and 0.72, predictability values (Q^2) above 0.89 and 0.83, model validity values above 0.70 and 0.80, and reproducibility values above 0.97 and 0.70 were obtained for DNA reduction and infectious virus titer responses, respectively (Fig. 1).

Analysis of significant model factors revealed that temperature,

Table 3
Filtration performance of primary clarification filters for fresh and frozen CCX.E10-derived material. The specifications of each filter are described in Table 1. Each filter processed 200 mL of fresh or frozen raw harvest containing rVSV-NDV.

		Device	IVP recovery (%)	Turbidity (NTU)	Turbidity reduction (%)	Pressure drop (psi)
Fresh	1.1	MC0HCC23L3	42	25.1	93	2.3
	1.2	MD0HCC23L3	24	5.2	98	5.6
	1.3	MCE5023CL3	100	125	64	4.3
Frozen	1.3	MCE5023CL3	100	46.2	44	3.0
	2.1	PP3 0.45 μm	100	16.0	81	4.4
	2.2	NF 0.22 μm	42	5.8	93	0.8

IVP: infectious virus particles; NTU: Nephelometric turbidity units.

Table 4
Performance of two clarification trains for CCX.E10-derived cell culture harvest containing rVSV-NDV.

	Operation step	IVP titer ($TCID_{50}$/mL)	IVP recovery (%)	Turbidity (NTU)	Turbidity reduction (%)	DNA (μg/mL)	Protein (mg/mL)	Pressure drop (psi)
Train 1	Harvest	3.2E + 08	–	400	–	14.7	3.2	–
	Nuclease treatment 1 h	2.4E + 08	75	390	2.5	3.2	2.6	–
	Filter 1.3	2.4E + 08	100	158	54	2.5	2.8	5.6
	Filter 2.1	3.2E + 08	100	52	87	1.4	2.3	0.8
Train 2	Harvest	3.2E + 08	–	471	–	18.5	1.8	–
	Sedimentation	3.2E + 08	100	83	82	18.6	2.2	–
	Nuclease treatment 1 h	3.2E + 08	100	n.d.	n.d.-	3.7	2.0	–
	Filter 2.1	3.2E + 08	100	40	92	2.0	2.8	0.3

IVP: infectious virus particles, NTU: Nephelometric turbidity units, n.d.: not determined, -: not available.

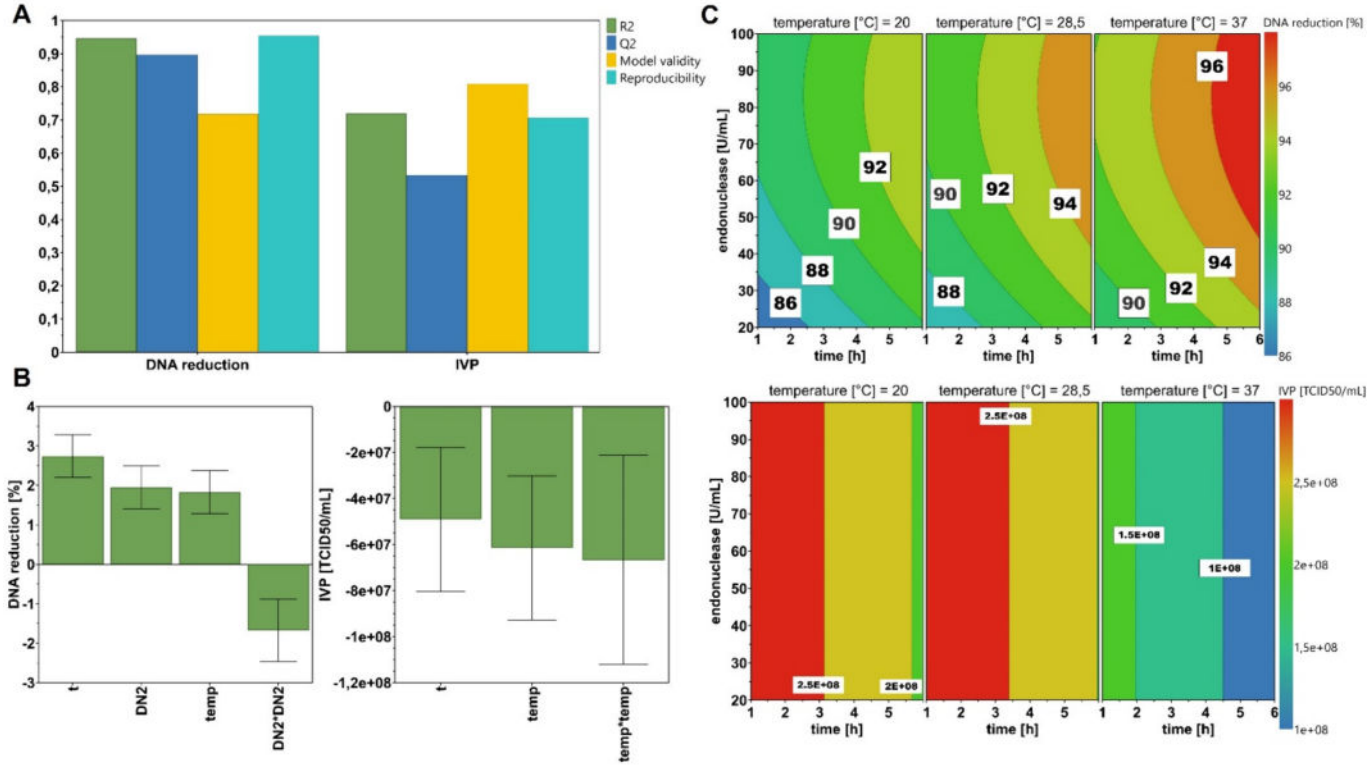

Fig. 1. Optimization of DNA digestion using a DoE approach. A CCF design with 3 factors and 3 responses was chosen to evaluate the DNA digestion of CCX.E10-derived cell broth, containing rVSV-NDV. (A) Summary of Fit plot using multiple linear regression analysis of responses: DNA digestion efficiency and infectious virus concentration. R^2: model fit, Q^2: predictability, validity: test of diverse model problems, reproducibility: variation within replicates. (B) Scaled and centered coefficients for DNA digestion efficiency and infectious virus concentration. Error bars represent the significance of the factor, while green bars represent the positive or negative impact of the factor on the response. (C) 4D contour plot of the interaction of the factors involved in the DNA digestion process. The influence of the incubation time (t), endonuclease concentration (DN2), and temperature (temp) on the responses DNA reduction and infectious virus titer (IVP) are shown.

incubation time, and endonuclease activity (quadatric effect) had a significant positive impact on DNA digestion. On the other hand, increases in temperature (quadratic effect) and incubation time had a significant negative effect on infectious virus concentrations. Response contour plots (Fig. 1C), visually represent the changes in DNA digestion efficiency and infectious virus titer over the parameter ranges. The plots indicate a high DNA digestion efficiency (>96 %) for long incubation times, high enzyme concentration, and high temperatures. However, infectious virus titers were negatively impacted by increasing the temperature and incubation time, regardless of the endonuclease concentration. Using cell-free supernatant resulted in similar DoE results, with high DNA digestion efficiencies (>96 %) for the highest temperature, enzyme concentration, and incubation time (data not shown). Using MODDE®'s optimizer function, the combination of factors resulting in the highest DNA digestion efficiency tolerating a loss of 10 % of infectious virus was identified. A DNA digestion efficiency of 92.5 % was predicted for both cell-free and cell containing harvest using an incubation time of 3.5 h at 28.5 °C with 60 U/mL endonuclease.

3.4. Screening of different AEX chromatography devices

Three devices were screened for the introduction of a chromatographic capture step: Capto DEAE resin, Mustang Q and Sartobind Q membranes. For these experiments, material from clarification train 1 was used. To select the best option for rVSV-NDV purification, infectious particles recovery yield and impurity clearance (total protein and DNA) were the parameters assessed with either gradient or step elution up to 2 M NaCl (145 mS/cm) (Fig. 2). A first strategy using gradient elution was used for all chromatographic devices investigated (Fig. 2-A). Three elution peaks were observed at 25 mS/cm, 55 mS/cm and 80 mS/cm corresponding to 20 %, 40 % and 55 % of elution buffer. Afterward, and based on this elution profile, a three-step elution strategy was performed with 0.4 M, 0.8 M and 2 M NaCl (Fig. 2-B). These two experiments were intended to be an initial screening, so different sample loads were used to preliminarily assess the membrane capacity. Additionally, Table S3 depicts the results in terms of recovery yield and impurity clearance. Comparing the recovery yields among the three evaluated chromatographic devices, Capto DEAE demonstrated the lowest virus recovery yield. Both membrane adsorbers enabled a high yield, however Sartobind Q outperformed Mustang Q by 23 % with 93 % over 70 %. Sartobind Q and Mustang Q demonstrated comparable purity results with over 98 % and 90 % for protein and DNA removal, respectively. However, Sartobind Q enabled the attainment of a slightly purer virus fraction with 99 % and 96 % of protein and DNA removal, respectively.

Across all three devices, peak 2 contained mostly eluted DNA impurities (30 % to 44 % across the three AEX matrices) with 40–50 mS/

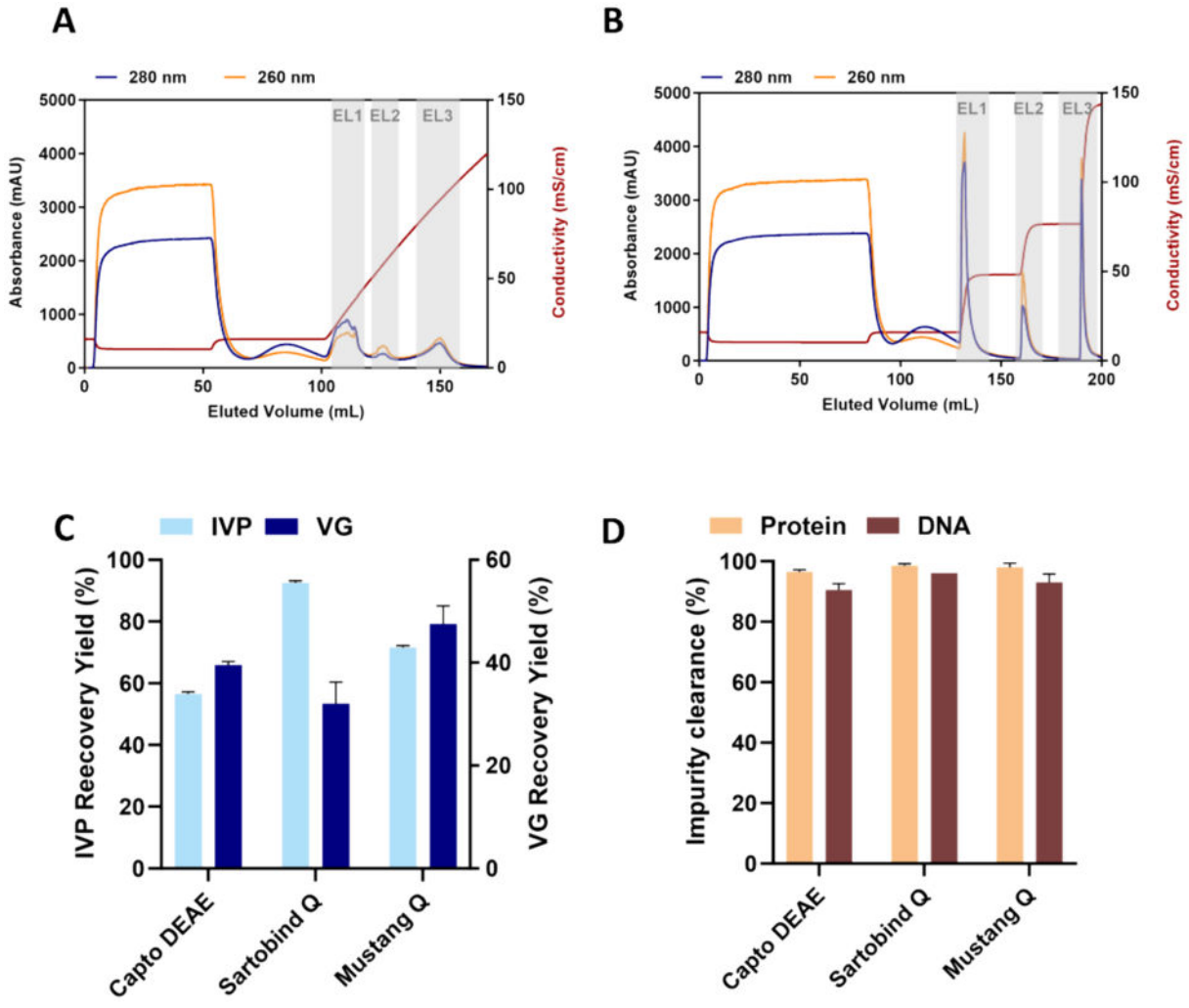

Fig. 2. Performance evaluation of three AEX chromatography devices for the purification of rVSV-NDV from CCX.E10-derived cell culture harvest. (A) Gradient elution strategy up to 2 M NaCl. (B) Step-wise elution strategy with 0.4 M, 1.2 M and 2 M NaCl; (C) Infectious viral particles (IVP) and viral genomes (VG) recovery yields in elution peak 3 with linear gradient elution strategy. (D) Impurity clearance (total protein and dsDNA) for the three AEX devices in elution peak 3 with linear gradient elution strategy. Values shown as the mean ± STD of a technical duplicate.

cm of conductivity, while in peak 3 the viral particles started eluting with 65–70 mS/cm. This difference is crucial to have a separation with good resolution and achieve a virus fraction with a high purity level. Thus, in further experiments the elution profile was adjusted in order to have two elution peaks (55 mS/cm and 90 mS/cm) – peak 1 with mostly DNA impurities and non-infectious viral particles, while peak 2 recovering most of the infectious viral particles.

Besides viral particle yield and impurities clearance, the ratio of viral genomes (VG) to IVP is an important parameter to assess. Interestingly, all three chromatography runs showed a decrease in the ratio VG to IVP in the virus peak, with 220, 98 and 224 for Capto DEAE, Sartobind Q and Mustang Q, respectively. In contrast, the other two elution peaks showed an increase in this ratio compared to the loading viral sample. This indicates an apparent enrichment of higher-quality particles as a high fraction of infectious particles is desired.

Both membrane adsorbers showed an efficient performance as capture steps for rVSV-NDV. However, Sartobind Q slightly outperformed Mustang Q, resulting in a purer viral fraction.

3.5. *Evaluation of chromatographic performance with addition of inorganic salts*

After AEX matrix selection, the effect of different inorganic salts on the purification of rVSV-NDV with Sartobind Q was assessed. For this, the different salts were added to the clarified feedstock at a final concentration of 100 mM and loaded onto the chromatographic column. For each run a respective set of buffers was used with the respective additive salt (sodium chloride, citrate, phosphate and carbonate). 50 mL of conditioned clarified material was loaded onto a Sartobind Q of 1 mL bed volume and eluted using a step-wise elution strategy with three steps as previously described. Fig. 3 shows the results of this with respect to viral recovery and clearance of impurities. A control was performed with rVSV-NDV clarified material conditioned with NaCl to normalize the chromatography feed to the same conductivity as the other conditions, around 24 mS/cm. Considering the elution profile of rVSV-NDV and impurities, two NaCl steps with 0.54 M and 1.2 M NaCl were performed. The conductivity of the first elution peak was slightly increased (from 0.4 M to 0.54 M NaCl) to enable a better peak resolution of the DNA impurities (55 mS/cm) from viral infectious particles eluting after (75 mS/cm).

For the control conditions, a recovery yield of 71 % and 34 % of IVP and VG was achieved, and 1.46 and 0.63 log reduction values (LRV) of total protein and DNA impurities were obtained, respectively. Two of the inorganic salts used as additives, citrate and phosphate, outperformed the control run in recovering viral particles, with yields of 86 % and 73 %, respectively. Also, an improvement was observed in terms of clearing impurities, with a considerable increase observed for both total protein and dsDNA contaminants. Citrate achieved 1.72 LRV and 1 LRV, while phosphate allowed for 1.47 LRV and 0.75 LRV for protein and DNA, respectively. Additionally, the analysis of VG recovery also revealed a low recuperation for both additives, with 24 % and 51 % for citrate and phosphate, respectively. In the case of carbonate, it was not possible to efficiently recover IVPs, with only a 20 % recovery yield. The poor performance also extended to the removal of impurities, with 1.42 and 0.45 LRV for protein and DNA, respectively. However, the VG yield for recovery was higher at 39 % compared to IVP, indicating a higher IVP to VG ratio.

To assess the impact of each inorganic salt on the virus' stability, the infectious titer was measured at different time points after storing the virus' eluted fraction of each chromatography run at 4 °C for 24 h and 48 h (Fig. 3-B). Carbonate was the only salt that negatively impacted viral infectivity with a 5-fold decrease at 48 h. The other salts, citrate and phosphate, showed no apparent loss of infectivity at the same time point with changes of around 1-fold, while the control run exhibited a

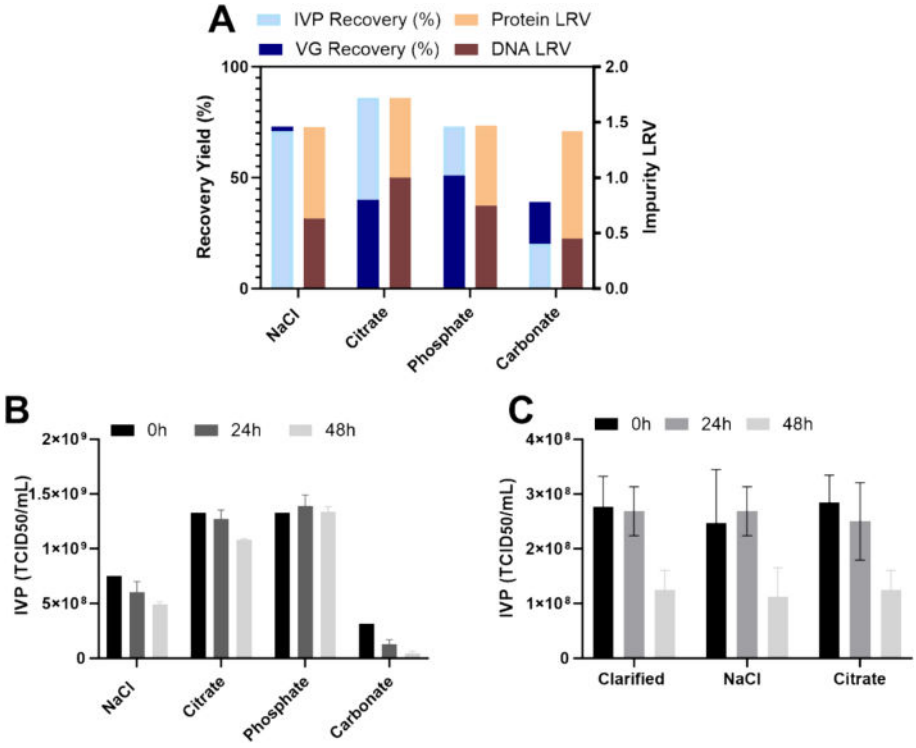

Fig. 3. Evaluation of the potential of inorganic salts for the purification of rVSV-NDV from CCX.E10-derived cell culture harvest. (A) Results of the Sartobind Q performance with different additive agents (conductivity control – NaCl; citrate; phosphate and carbonate in terms of viral recovery (IVP and VG) and impurities clearance (total protein and dsDNA). (B) Stability evaluation of the different elution fractions at 4 °C at different time points 0 h, 24 h and 48 h. (C) Stability evaluation of rVSV-NDV clarified material conditioned with 40 mM of NaCl or 100 mM citrate at 4 °C at time points 0 h 24 h, and 48 h. Values shown as the mean ± STD of a technical duplicate.

1.5-fold reduction. Fig. 3-C shows a similar stability evaluation but of the chromatography load samples conditioned with either NaCl or citrate. When compared with the only clarified rVSV-NDV material, with only 5 % (v/v) sucrose as additive, no loss of infectivity was observed at such conditions after 24 h at 4 °C. However, after 48 h a decrease of around two-fold was observed for all the conditions.

Given all of these results, citrate was selected as the preferable chromatographic additive for the purification of rVSV-NDV using the Sartobind Q membrane.

3.6. Quality assessment of purified rVSV-NDV

Virus sample purified with Sartobind Q was separated into two elution fractions with citrate as a chromatography additive. Subsequently a more detailed analytical characterization was conducted using CE-SDS with a fluorescence detector and TEM for these two elution fractions (Fig. 4).

Only 3 % of infectious particles were recovered from elution fraction 1, while, 86 % were recovered from elution fraction 2. However, a different profile can be observed for VG with 40 % and 24 % of recovery for elution fraction 1 and 2, respectively. This opposite profile is

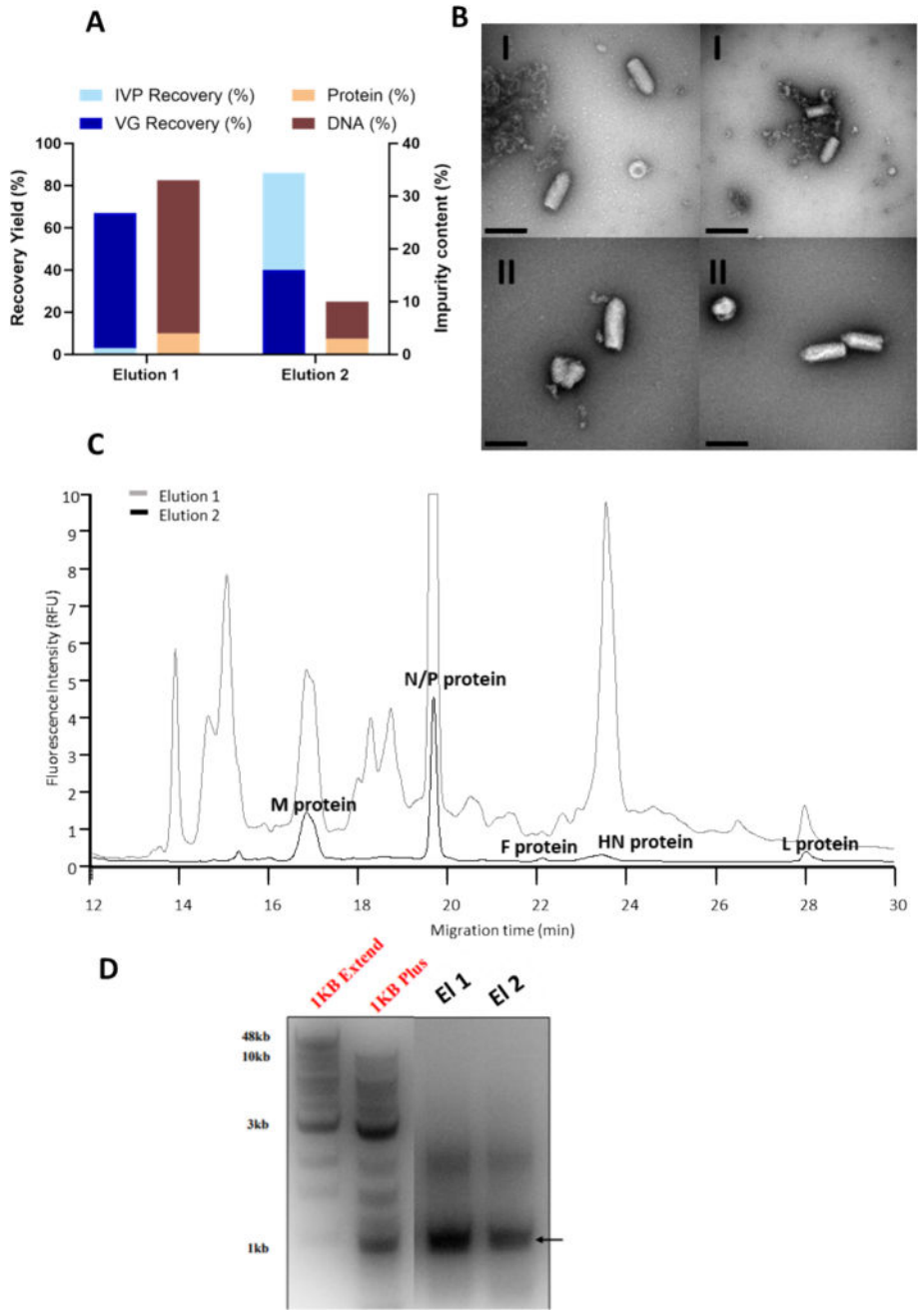

Fig. 4. Comparison and characterization of the AEX Sartobind Q elution profile with citrate additive. (A) Infectious viral particles (IVP) and viral genomes (VG) recovery yields in elution peak 1 and 2. (B) TEM analysis I – Elution peak 1; II – Elution peak 2 (scale of 200 nm). (C) CE-SDS with LIF detector profile of both elution peaks (Elution 1 – grey and Elution 2 – black) (D) Agarose gel analysis of the single primer cDNA synthesis and PCR amplification for the detection of defective-interfering (DI) genome in both elution peaks. Both methodologies (CE-SDS and TEM) support the findings from viral and impurity content using the standard analytics. Elution peak 1 contains non-infectious viral particles and product-related impurities such as DNA fragments, while elution peak 2 contains a purer fraction of mainly infectious viral particles.

observable by comparing both recovery bars in Fig. 4-A, which indicates elution peak 2 has a lower VG to IVP ratio. In terms of purity, the second chromatography peak also shows a clearer profile with 10 % of DNA, while the first peak exhibits 33 % of DNA present.

Comparison of the electropherograms (Fig. 4-C) shows a less clean profile for elution 1, which makes it difficult to identify the viral particles as compared to elution 2. However, in terms of the presence of physical viral particles, both elutions appear comparable and show similarity as seen in the TEM analysis presented in Fig. 4-B.

In images of Elution 1 several aggregates of small fragments that seem to even aggregate with viral particles can be identified. This can be explained by the higher DNA content in this fraction (33 % of the loaded sample).

Additionally, an agarose gel of the resulting DIP PCR was performed in order to potentially identify the presence of DIPs. A band around 1 kb was expected, since it is the known genome size of rVSV-NDV (data not shown). Comparing both elution fractions (Fig. 4-B) the said band seems more intense in elution peak 1, corroborating the apparent enrichment of DIPs in this fraction.

3.7. Evaluation of dynamic binding capacity (DBC)

The DBC of Sartobind Q was determined from the ratio of total particles (TP) and IVP in the flow-through in relation to the concentration load at different time points during 200 MV of clarified harvest. For this study, TP was measured using Nanoparticle tracking analysis (NTA). To determine the impact of citrate as a chromatography additive, binding capacity studies were performed with 100 mM citrate addition to the clarified material and a control condition with only conductivity equilibration, as previously compared (Fig. 5). Here, clarified material was used with a concentration of 1.3×10^8 $TCID_{50}$/mL and 3.3×10^{10} TP/mL and loaded at 5 MV/min on a 1 mL Sartobind Q.

For both conditions, the curves exhibit the typical sigmoidal curve for either TP or IVP, with the exception of the IVP with NaCl condition (Fig. 5-A), which had a more linear tendency revealing an earlier breakthrough. From the results obtained, the DBC at 10 % breakthrough was 1.9×10^{12} and 2.4×10^{12} TP, and 1.0×10^{10} and 7.1×10^9 IVP for citrate and NaCl conditions, respectively. This result corroborates the previously observed findings, where an improvement in the chromatography performance with the addition of some inorganic salts at pH 8.0 was observed.

The impurity profile was also analyzed for both conditions in the different FT fractions (Fig. 5-B). For both, the protein breakthrough curve showed a hyperbolic shape, revealing low protein adsorption onto AEX matrix. However, in comparison, the citrate condition reached a higher maximum plateau, meaning that lower non-specific binding was occurring. For DNA breakthrough, each condition showed a different profile. When NaCl was used, the curve showed a sigmoidal shape, whereas citrate resulted in a more accentuated curve. This indicates DNA impurities were binding less and breaking through earlier in the latter condition. This might explain the higher dynamic capacity for infectious particles. In the end, the addition of citrate enhanced Sartobind Q efficiency in purifying the fusogenic oncolytic virus of this work.

3.8. Implementing a complete purification strategy for rVSV-NDV manufacturing

After the scaled-down scouting experiments shown in this study, a complete purification process was set-up, focusing on the capture step with chromatography, followed by a tangential flow filtration (TFF) step for additional concentration and diafiltration, and finally a sterilizing filtration step. For this, 250 mL of clarified rVSV-NDV material was conditioned with 100 mM citrate and loaded onto a 3 mL Sartobind Q. The results of this process are depicted in Table 5 for viral recovery and impurity clearance. In the capture step, a recovery yield of 80 % of IVP was obtained, while only 42 % of VG were recovered, corroborating what was previously obtained with an apparent enrichment of infectious particles in the elution fraction. Total protein impurities were mostly removed in the chromatographic step with 98 %, corresponding to a 1.63 LRV. Regarding the DNA removal, a removal of 83 % was achieved, representing 0.72 LRV, slightly lower than the obtained in the previous scale-down scouting.

After chromatography, the rVSV-NDV eluted fraction with 1.2 M NaCl from the chromatographic step was diluted 4x with equilibration buffer containing 100 mM citrate and loaded onto TFF devices to concentrate and formulate. The selected TFF parameters were 750 kDa cut-off membrane, 2500 s^{-1} shear rate and a transmembrane pressure (TMP) of 0.3 bar. The TFF only recovered 47 % of IVP from the eluted fraction. During process development, a different TFF run was conducted at a higher shear rate (5500 s^{-1}) and a similar recovery yield of 56 % was obtained (data not shown). On the other hand, no loss of either IVP or VG was observed in the sterilizing filtration with the EKV filter, revealing to be a successful strategy for this enveloped virus.

The global recovery yield of IVP was 64 %, while that of VG was 17 %. These results confirm the high selectivity of the developed process for infectious particles, allowing a substantial reduction in the ratio of non-infectious to infectious particles achieving a ratio of 40 after the sterile filtration.

Additional characterization of in-process samples was conducted by CE-SDS with LIF detector (Fig. 6-A) and by TEM (Fig. 6-B). Using the first technique, it was possible to identify the specific viral proteins known to belong to rVSV-NDV. Through extrapolation from a calibration curve from a molecular weight marker (Figure S2), it was possible to confirm the expected MW of structural construction of rNDV-VSV, composed by

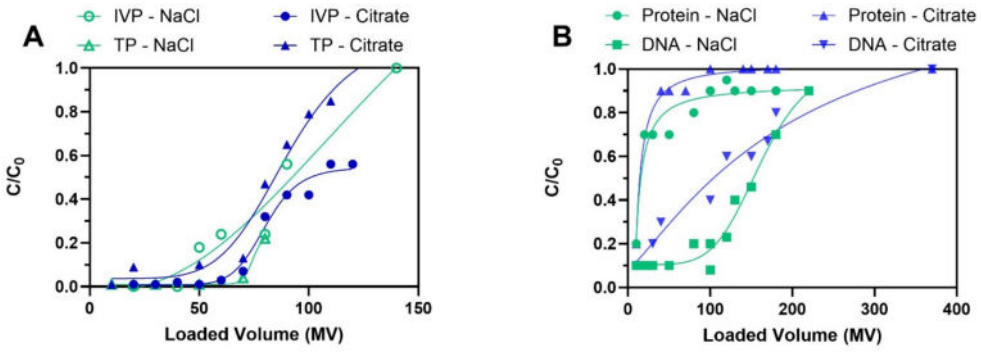

Fig. 5. Representation of the breakthrough curves (BC) for Sartobind Q membrane with rVSV-NDV feedstock conditioned with 40 mM sodium chloride (blue) and 100 mM citrate (green). The load velocity was 5 MV/min. (A) BC of viral particles where C is either the total (TP – triangles) or infectious particles (IVP – circles) concentration of flow-through fractions, and C_0 is the virus concentration of loaded feedstock material. TP was determined by Nanoparticle Tracking analysis (NTA) and IVP concentration by $TCID_{50}$ assay. (B) BC of impurities (total protein and dsDNA).

Table 5
Results for the complete purification process of rVSV-NDV. *Note: Elution peak 2 was diluted 4x times in equilibration buffer.

			Total					% of the Total			
	Fraction	V (mL)	IVP ($TCID_{50}$)	VG	VG/IP ratio	Protein (mg)	DNA (µg)	IVP	VG	Protein	DNA
Chromatography	**Load**	270	7.47E + 10	1.13E + 13	152	314.13	254.42	100	100	100	100
	Pool FT	300	8.99E + 08	7.80E + 11	867	285.07	12.32	1	7	91	5
	EL1	10	2.47E + 09	3.30E + 12	1336	6.90	98.61	3	29	2	39
	EL2*	60	6.00E + 10	4.74E + 12	79	7.32	43.93	80	42	2	17
TFF	**Retentate**	16	2.85E + 10	1.92E + 12	67	5.63	22.79	47	41	77	52
	Permeate	98	3.10E + 02	0.00E + 00	0	1.83		0	0	25	11
Sterile Filtration	**Final Drug substance**	12	4.80E + 10	1.92E + 12	40	3.53	16.54	100	100	63	73
Overall Yields (%)								**64**	**17**	**99**	**93**

IVP: infectious virus particles; VG: viral genomes, FT: flow-through, EL: elution

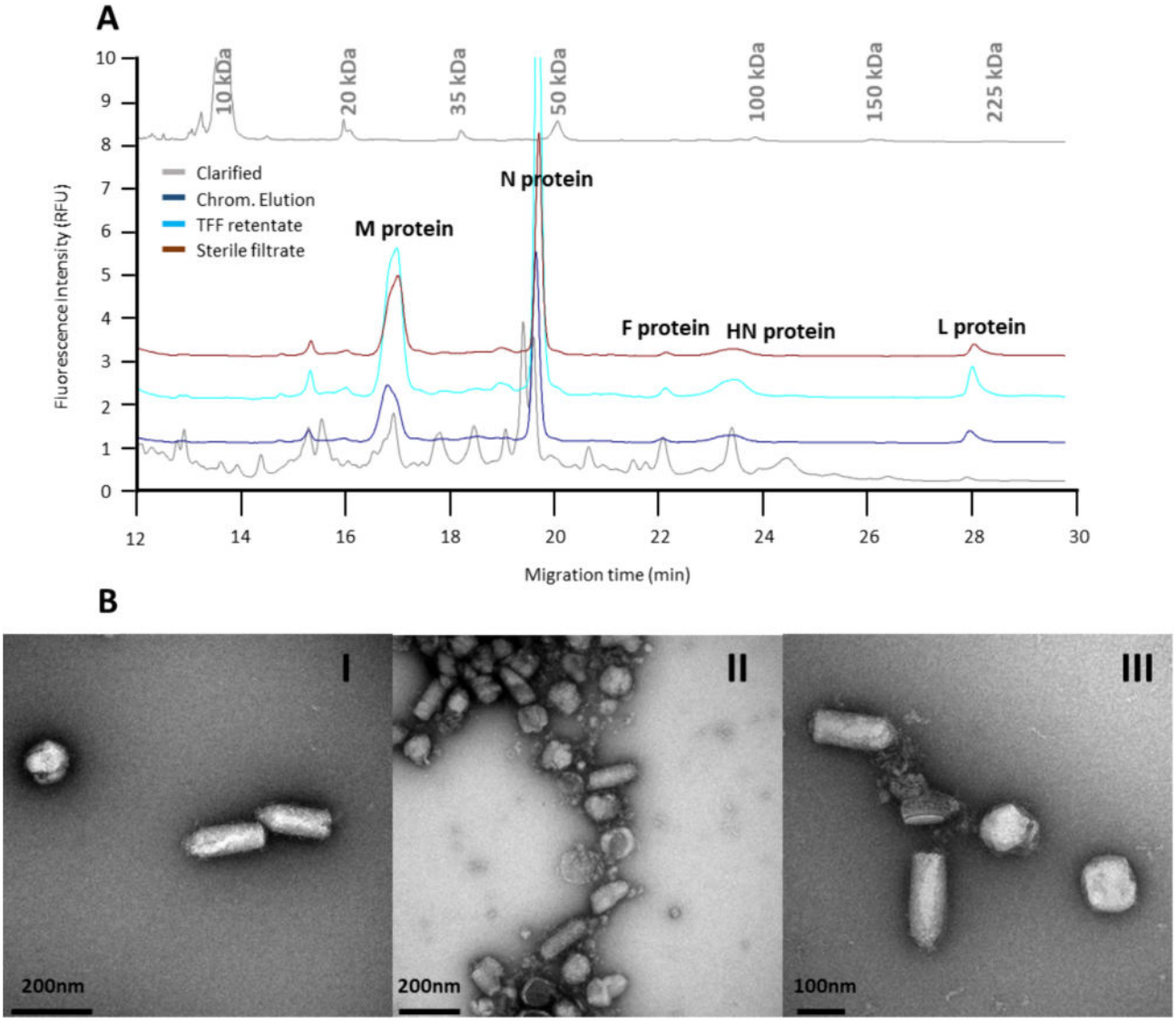

Fig. 6. Final product and in-process sample characterization from complete purification process of rVSV-NDV. (A) Protein profile evaluation by capillary electrophoresis with laser-induced detector (LIF). (B) Analysis by transmission electron microscopy (TEM) of I – Sartobind Q virus' elution fraction; II – TFF Retentate; III – Final product after sterile filtration.

protein N (42 kDa), M (23 kDa), L (256 kDa) and enveloped proteins F (66 kDa) and HN (82 kDa).

rVSV-NDV was analyzed with TEM to identify the impact of the different operation units integrated into the process on vector morphology and purity. Samples after the chromatography, TFF and sterilizing filtration were analyzed. Bullet-shaped particles with a size of around 200 nm to 50 nm were identified in all of them. Additionally, there were round-shaped particles present in close proportion with a diameter of approximately 100 nm. Moreover, the clear background confirms the purity after the chromatography step. This is also supported by CE-SDS results, where the low peaks present in the clarified line in the electropherogram disappear further in the next in-process

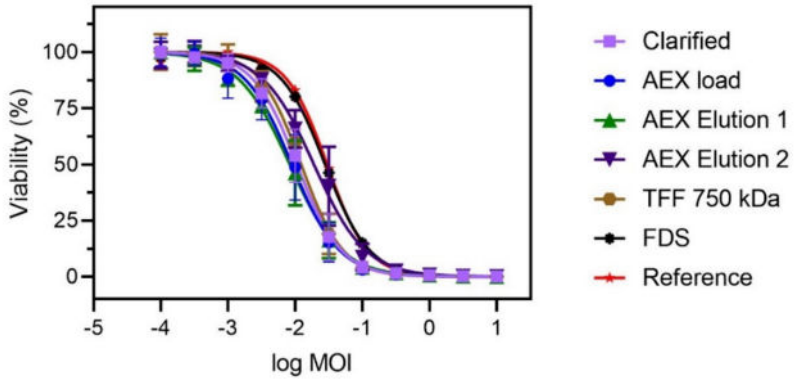

	Clarified	AEX load + 100 mM Citrate	AEX Elution 1	AEX Elution 2	TFF 750 kDa Retentate	FDS	Reference
Log IC_{50}	-1.975	-2.049	-2.082	-1.723	-1.912	-1.555	-1.527
IC_{50}	0.011	0.009	0.008	0.0189	0.0123	0.0279	0.0297

Fig. 7. Comparison of oncolytic viral potency values for rVSV-NDV in different downstream unit operation steps. rVSV-NDV samples generated after clarification (purple square), addition of 100 mM citrate (AEX load, blue circle), AEX Elution 1 (green triangle) and Elution 2 (purple triangle), TFF (brown hexagon), and finale sterile filtration (FDS, black asterisk) were added to Huh7 human cancer cells, and viabilities were determined 48 hpi by CellTiter Glo assay (Promega). rVSV-NDV produced in CCX.E10 cells and purified on sucrose-gradients was used a reference. IC_{50} and log IC_{50} values were determined from dose-response curves, following non-linear regression analysis. All values are reported as the mean of technical triplicates with N = 3.

samples (Fig. 6-A).

Finally, oncolytic potency was evaluated to identify the impact of the different unit operations and compared to sucrose-gradient purified material of a reference culture. As indicated in Fig. 7, all samples displayed a similar oncolytic potential in human cancer cells (Huh7).

4. Discussion

4.1. Optimization of DNA digestion and clarification step

Clarification and endonuclease digestion are usually the first critical unit operations in most downstream processes of viral and oncolytic vectors [23]. Endonuclease treatment before filtration has been shown to increase filter capacities by reducing the viscosity of the cell broth and preventing competitive binding of nucleic acids to the filters. Optimal clarification trains should remove cells, cell debris, and particulate impurities, thus efficiently reducing turbidity while maintaining a high product recovery [24]. Due to the well-established stabilizing effect of sucrose on infectious virus titer, all crude harvests were supplemented with 5 % sucrose [25–27].

After the endonuclease treatment, a screening of primary and secondary clarification steps was evaluated for rVSV-NDV separation from the other cell culture-based impurities. Initially, a set of filters composed of different materials, with pores ranging from 10 to 0.2 μm, were investigated by evaluating turbidity reduction and IVP recovery (Table 3 and 4). From the analysis of the different results, filters 1.1 and 1.2 presented the lowest turbidity values (25 and 5 NTU) with an associated load of 87 L/m^2 in the initial screening, however, recovery of infectious virus titer was low (42 and 24 %). Filter 1.3 was less retentive, as shown by the higher turbidity value (125 NTU), however, all IVPs were recovered. Both filters, 1.1 and 1.2, are multilayer depth filters designed for primary clarification directly from the bioreactor. The combination of cellulose-containing layers with diatomaceous earth (DE) −containing layers allowed a more efficient reduction of turbidity compared to a single layer of cellulose filter media (filter 1.3), as particles were adsorbed by a combination of hydrophobic and electrostatic interactions. However, the positive charge of DE might have resulted in the adsorption of negatively charged rVSV-NDV, resulting in lower recovery of infectious virus [28,29]. Therefore, filter 1.3 was selected for subsequent experiments, and an additional secondary clarification step was performed to further remove colloidal material and cellular debris that were not retained in the preceding filtration (Table 4). The addition of filter 2.2 resulted in a further reduction of turbidity by 81 % to 16 NTU without any loss of infectious virus at an associated load of 87 L/m^2. The inert nature of polypropylene, characterized by a lower surface tension energy compared to other materials e.g. polyethylene sulfone, polystyrene, or polyethylene seems to be beneficial for clarification of virus-containing supernatant [30,31]. Final sterile filtration using filter 2.2 resulted in a final yield of 42 % with turbidity values below 10 NTU, suggesting that the polyether sulfone material did adsorb some of the IVPs and thus was not selected for initial clarification.

In the next step, filters 1.3 and 2.1 were selected for an investigation at a larger scale using material produced in 1 L STRs. Additionally, an alternative clarification train for material produced in a 3 L STR was evaluated, using sedimentation at room temperature for 24 h for primary clarification followed by filtration with filter 2.1. Surprisingly, the endonuclease digestion step only resulted in a 78–80 % reduction of DNA for both clarification trains. As the endonuclease digestion step was optimized for rVSV-NDV-containing supernatant produced in HEK293 cells using a different medium, it seemed that the presence of cells or supplemented Freestyle™293 Expression medium could interfere with DNA digestion. Nevertheless, clarification train 1 resulted in final turbidity reduction and DNA reduction of 87 % (52 NTU) and 90.5 %, respectively, with a complete recovery of infectious virus particles. Both filters allowed clarification of 1.4 L of digested harvest material without clogging, achieving a capacity of 610 L/m^2 for filter 1.3 and 58 L/m^2 for filter 2.1. Clarification train 2 reduced solution turbidity and DNA concentration by 92 % (40 NTU) and 89.2 %, while also allowing a complete recovery of infectious virus particles. However, after removal of the supernatant clarified by sedimentation, only 2 L of the initial 2.5 L cell broth could be recovered and further processed, resulting in a final capacity of 83 L/m^2. Compared to centrifugation, which requires high capital investment, sedimentation is cheap and easy to operate and potentially more easily scalable. Although a loss of IVPs during the sedimentation step was prevented by the addition of 5 % sucrose, 20 % of the total volume was lost, rendering this option uneconomical.

For DNA digestion optimization, incubation time, endonuclease concentration, and incubation temperature were identified as significant factors affecting DNA digestion in terms of digestion efficiency and recovery of infectious virus particles. Despite a large design space (data

not shown), it should be considered that higher temperatures and increased incubation time decrease the infectious titer. Loss of infectivity at higher temperatures and incubation periods is well known, particularly for enveloped RNA viruses [32]. Presence of intact cells did not affect the DNA digestion efficiency. The optimal set-point identified with the optimizer function of MODDE suggests using an endonuclease concentration of 60 U/mL combined with a moderate incubation time (3.5 h) at moderate temperatures (28.5 °C). Applying those DNA digestion parameters, the predicted DNA digestion efficiency of 92.5 % clearly surpasses the efficiencies reached in the clarification trains 1 and 2. However, endonuclease concentrations of 35 U/mL have been attributed to up to 32 % of cost per dose of viral vectors. Therefore, the increase in efficiency by high endonuclease concentrations should be weighed against the additional process costs. [33].

4.2. Developing a robust purification scheme for rVSV-NDV

Currently, methods such as density gradient ultracentrifugation and size exclusion chromatography are the standard operations for the purification of clinical grade OVs [1]. However, these processes are time-consuming and are not the preferred choice with respect to large-scale manufacturing. Anion exchangers were chosen for the purification of rVSV-NDV from clarified feedstock given the virus surface properties, since NDV glycoproteins (fusion protein (F) and hemagglutinin neuraminidase (HN)) have a negative net charge at physiological pH [29,34]. To optimize the AEX step, a small scouting experiment was conducted assessing the recovery yield and purity from the elution fractions from Capto DEAE, Mustang Q and Sartobind Q. From a gradient elution, a two-step elution strategy (0.54 M and 1.2 M) was optimized and employed for further purifications. Sartobind Q membrane was selected as the best candidate, achieving a maximum of 93 % of IVP at small-scale (1 and 3 ml). The other candidates, Capto DEAE and Mustang Q, achieved comparable purity profiles but lower recovery yields of 56 % and 71 %, respectively. In the literature, several strategies are reported using both competitors for the purification of enveloped viruses [35–37]. Upon analyzing the structural differences between Sartobind Q and Mustang Q membranes, Sartobind Q has a larger pore size of 3 μm, compared to 0.8 μm for Mustang Q. However, this factor by itself might not account for the higher performance observed in the former. Overall, the impact of membrane structure apart from pore size remains unclear and requires further investigation [38]. Additional factors such as pH and conductivity are known to strongly impact on anion exchange media. Thus, after selecting the best AEX device, we next tried to improve the chromatography performance by using the interference of additional additives. In this study, we evaluated the performance of inorganic salts that have different protonation states, such as citrate, carbonate, and phosphate. Depending on the pH at operation, these specimens could become more negatively charged, thereby binding more strongly to the AEX matrix. A similar strategy was already employed for the purification of NDV, where adding inorganic salts improved the protein removal [39]. Surprisingly, in the present study, the three evaluated AEX matrices revealed the same elution pattern, showing the DNA impurities eluting before the virus fraction. This profile is uncommon to what is described in the literature for AEX purification strategies, where usually a co-elution is observed [11,40]. Nevertheless, scouting experiments were conducted in 1 mL Sartobind Q to further optimize its performance, by tackling an expected interference in the binding of biomolecules to the chromatographic matrix. It was anticipated that the negatively charged additives would bind to the adsorber, leading to an early elution of the analytes. This would result in a higher resolution between negatively charged impurities and the desired viral particles. At pH 8.0, 100 mM of citrate, phosphate, and carbonate (which show 3, 2, and 1 ion forms, respectively) were used since the virus is stable at pH 8.0 [41,42]. Citrate was the additive that demonstrated the best performance in the capture step, allowing the recovery of 86 % of IVPs and achieving protein and DNA clearance in 1.72 and 1.00 LRV, respectively. Moreover, information on short-term stability (up to 48 h) was collected on the chromatography loading material, and elution fraction was collected by verifying the IVP content after 4 °C storage. Citrate was shown to not interfere with virus stability in any of the conditions evaluated. Additionally, citrate positively impacted chromatography performance, increasing the DBC of Sartobind Q by 1.5-fold specifically for IVP. There is no process reported in the literature for this chimeric virus, although comparisons can be made with its parental viruses (VSV or NDV), since they are similar in size, and this factor strongly impacts on DBC. Santry et al. reported a maximum $DBC_{10\%}$ of 1.5×10^{10} $TCID_{50}$/mL for the purification of rNDV using an AEX membrane [39]. Our chromatography showed a $DBC_{10\%}$ of 1.0×10^{10} $TCID_{50}$/mL for purifying rVSV-NDV, which is comparable with the described method.

After chromatography, TFF is typically applied for extra concentration and/or product formulation [43]. A TFF step using hollow fiber (HF) was evaluated, showing a 47 % recovery yield. However, no correlation between shear rate and recovery yield was observed. The use of HF to concentrate and formulate similar enveloped viruses is described in the literature, and given the fragility of this class of viruses, usually low recovery yields are obtained. Makovitzki et al. reported 40 % of recovery yield for a rVSV target using a HF membrane with the same MWCO of 750 kDa as used in this study [44]. Further optimization of the number of diafiltrations in the TFF step might be required to guarantee future impurity content within guidelines for clinical application.

To produce clinical grade OVs, a final sterile filtration is required. Moreover, this step could be critical especially in the manufacturing of enveloped viruses, which are characterized by their large size, and are often subject to significant losses in this step, impacting the overall yield of the manufacturing process [45]. Often, a complete aseptic process is necessary if sufficient yields after sterile filtration cannot be achieved, leading to substantially higher production costs and severe limitations in the number of GMP facilities that can accommodate such a process. Fortunately, from the filters evaluated for rVSV–NDV, the Supor EKV filter allowed complete recovery of infectious virus particles, which is a great advantage for a future GMP production process.

4.3. Quality assessment of purified rVSV-NDV

As of now, there are no specific regulatory guidelines in place outlining the production and characterization of OVs for clinical applications [6]. However, as they are classified as gene therapy products by the EMA and FDA, the respective guidelines can be assumed [14,46,47]. Compliance with these regulations mandates the achievement of three key goals in the production: high virus concentration yields to allow small volume doses, high levels of purity, and maintenance of high potency and quality [48]. In a previous phase I VSV-GP OV clinical study, dose escalations from 5.0×10^7 to 5.0×10^{10} infectious units/dose were investigated [49]. If a similar clinical trial design is used for rVSV-NDV, the final rVSV-NDV yield of 4.0×10^9 $TCID_{50}$/mL would allow for small-volume doses of 0.21–210 μL kg^{-1} bodyweight when injected intravenously or intraperitoneally. Assuming a similar minimum and maximum dose as for oncolytic VSV-GP, our combined up-and downstream process would enable the production of 5–4800 doses per 1 L culture cultivation. Furthermore, with respect to the specified dose, purified rVSV-NDV samples exhibited concentrations of 0.02–17.24 μg/dose of double-stranded DNA (dsDNA) and 0.0–3.68 mg/dose of total protein. Despite the batch release criteria stipulating levels below 10 ng of host cell DNA (hcDNA) per dose and less than 100 ng/mL of host cell protein (HCP), currently there is no generic quail cell HCP ELISA on the market, but alternative methods based on mass spectrometry (LC-MS) are in development. However, following endonuclease treatment, the presence of protein and DNA decreased by magnitudes of 89 and 15-fold, respectively. Optimization of diafiltration cycles could be pursued to further eliminate additional impurities, thereby ensuring compliance with regulatory requirements [9].

Ratios of non-infectious to infectious virus particles (VG/IVP) are another critical quality parameter for virus-based therapeutics, however, universal ratios for all virus types are not available [50]. For oncolytic adenovirus stocks, VG/IP ratios range from 13 to 65, for oncolytic measles virus stocks VG/IVP ratios below 50 are targeted [1,51]. For recombinant VSV-based vaccine constructs, VG/IVP ratios of clinical products can range from 6 for rVSV-COV2 [52], 100 for rVSV-EBOV [52], to 4384 for rVSV-HIV [53]. Similar to the three rVSV-variants, rVSV-NDV contains heterologous glycoproteins (surface proteins from NDV) responsible for cell entry. As the intracellular replication and final assembly processes of these proteins vary, differences in the quantity of functional rVSV particles and VG/IVP ratios are expected [53]. Nevertheless, achieved VG/IVP rVSV-NDV ratios of 40 are within the range of other clinical OV preparations and below the EMA recommended ratio of 50 [1].

Capillary electrophoresis already proved to be a valuable methodology for the characterization of enveloped viruses such as rVSV-NDV [22]. Thus, this technique was used for qualitative assessment of the chromatography fractions searching for the core viral proteins (M, N HN, F and L proteins), as well as low MW protein impurities. Additional visualization with TEM imaging confirmed the high purity after final sterile filtration. Besides confirmation of the prototypical bullet shape of VSV-particles [54], truncated circular particles with a diameter of 70–100 nm were identified. Similar particles have been previously identified as defective interfering particles (DIPs). DIPs are characterized as non-infectious particles, which are unable to replicate independently, and interfere with standard virus replication [55,56]. The identified VG/IVP ratios should therefore be recognizable in the TEM images as an accumulation of round particles that are consistent in size with previously reported VSV DIPs in comparison to bullet-shaped rVSV-NDV. However, the TEM images acquired did not show a conclusive relative quantification of these two kind of particles in the two elution fractions. Instead, showing the presence of both particles in each of the said fractions.

We previously showed that sucrose gradient-purified rVSV-NDV virus produced in perfusion mode showed increased oncolytic potency in Huh7 cells compared to unpurified virus [57]. As the starting material used here had already been DNA digested and purified, the majority of DNA and protein that potentially could interfere with the infectivity of the virus and thus the potency had already been removed, resulting in similar potency values across all unit operations. Moreover, the final potency was in line with material purified on sucrose-gradients.

In summary, a complete purification process for rVSV-NDV was developed and thoroughly evaluated. While this process was not carried out in a manufacturing facility, all materials used are scalable and available in GMP grade and should be easily transferred to a GMP environment. Therefore, based on our knowledge, this work represents a significant step towards the production and purification of rVSV-NDV, which could facilitate the translation of fusogenic OVs for clinical use.

Ethics approval

This article does not contain any studies with human participants or animals performed by any of the authors.

Funding

This work was funded by Fundação para a Ciência e Tecnologia/Ministério da Ciência, Tecnologia e Ensino Superior (FCT/MCTES, Portugal) through national funds to iNOVA4Health (UIDB/04462/2020 and UIDP/04462/2020), the Associate Laboratory LS4FUTURE (LA/P/0087/2020) and project PTDC/BTM-ORG/1383/2020; R.F is recipient of a FCT PhD fellowship PD/BD/2020.06003.

CRediT authorship contribution statement

Rita P. Fernandes: Writing – review & editing, Writing – original draft, Project administration, Methodology, Investigation, Conceptualization. **Sven Göbel:** Writing – review & editing, Writing – original draft, Project administration, Methodology, Investigation, Conceptualization. **Manfred Reiter:** Writing – review & editing, Resources. **Alexander Bryan:** Resources, Methodology. **Jennifer Altomonte:** Writing – review & editing, Conceptualization. **Yvonne Genzel:** Writing – review & editing, Supervision, Funding acquisition, Conceptualization. **Cristina Peixoto:** Writing – review & editing, Supervision, Funding acquisition, Conceptualization.

Declaration of competing interest

The authors declare the following financial interests/personal relationships which may be considered as potential competing interests: J. Altomonte (WO 2017/198779) holds a patent for the development and use of rVSV-NDV as an oncolytic therapy of cancer and is co-founder of Fusix Biotech GmbH, which is developing the rVSV-NDV technology for clinical use. M. Reiter is an employee of Nuvonis Technologies, which owns the CCX.E10 cells.

Data availability

Data available in article supplementary material. Additional data is available on request from the authors. The data that support the findings of this study are available from the corresponding author, Cristina Peixoto, upon reasonable request.

Acknowledgment

The authors would like to thank ProBioGen for providing the adherent AGE1.CR.pIX cells. The authors acknowledge. Teresa Krabbe for guidance, diligent help, and skilled execution of the oncolytic potency assay. The authors also acknowledge Erin M Tranfield and Ana Laura Sousa from the Electron Microscopy facility, IGC, for the microscopy support.

Appendix A. Supplementary data

Supplementary data to this article can be found online at https://doi.org/10.1016/j.seppur.2024.128769.

References

[1] G. Ungerechts, S. Bossow, B. Leuchs, P.S. Holm, J. Rommelaere, M. Coffey, R. Coffin, J. Bell, D.M. Nettelbeck, Moving oncolytic viruses into the clinic: clinical-grade production, purification, and characterization of diverse oncolytic viruses, Mol. Ther. Methods Clin. Dev. 3 (2016) 1–12.
[2] K.G. Anderson, D.A. Braun, A. Buqué, et al., Leveraging immune resistance archetypes in solid cancer to inform next-generation anticancer therapies, J. Immunother. Cancer (2023), https://doi.org/10.1136/jitc-2022-006533.
[3] P.F. Ferrucci, L. Pala, F. Conforti, E. Cocorocchio, Talimogene laherparepvec (T-vec): An intralesional cancer immunotherapy for advanced melanoma, Cancers (basel) 13 (2021) 1–14.
[4] Jane Flint VRRGFRTHAMS, Principles of virology, 5th ed. ASM Press, Washington, DC, 2020.
[5] A. Sarah, J. Melanie, B.S. J, et al., A Novel Chimeric Oncolytic Virus Vector for Improved Safety and Efficacy as a Platform for the Treatment of Hepatocellular Carcinoma, J. Virol. 92 (2018), https://doi.org/10.1128/jvi.01386-18.
[6] T. Yamaguchi, E. Uchida, Oncolytic Virus: Regulatory Aspects from Quality Control to Clinical Studies, Curr. Cancer Drug Targets 18 (2017) 202–208.
[7] J. de Sostoa, V. Dutoit, D. Migliorini, Oncolytic viruses as a platform for the treatment of malignant brain tumors, Int. J. Mol. Sci. 21 (2020) 1–22.
[8] N. Singh, C.L. Heldt, Challenges in downstream purification of gene therapy viral vectors, Curr. Opin. Chem. Eng. (2022), https://doi.org/10.1016/j.coche.2021.100780.
[9] D. Loewe, H. Dieken, T.A. Grein, D. Salzig, P. Czermak, A Combined Ultrafiltration/Diafiltration Process for the Purification of Oncolytic Measles Virus, Membranes (basel) (2022), https://doi.org/10.3390/membranes12020105.

[10] S. Firquet, S. Beaujard, P.E. Lobert, F. Sané, D. Caloone, D. Izard, D. Hober, Survival of enveloped and non-enveloped viruses on inanimate surfaces, Microbes Environ. 30 (2015) 140–144.
[11] T. Rogerson, G. Xi, A. Ampey, J. Borman, S. Jaroudi, D. Pappas, T. Linke, Purification of a recombinant oncolytic virus from clarified cell culture media by anion exchange monolith chromatography, Electrophoresis 44 (2023) 1923–1933.
[12] S. Gautam, D. Xin, A.P. Garcia, B. Spiesschaert, Single-step rapid chromatographic purification and characterization of clinical stage oncolytic VSV-GP, Front. Bioeng. Biotechnol. (2022), https://doi.org/10.3389/fbioe.2022.992069.
[13] A.R. Swartz, Y. Shieh, A. Gulasarian, E. Curtis, C.F. Hofmann, J.B. Baker, N. Templeton, J.W. Olson, Glutathione affinity chromatography for the scalable purification of an oncolytic virus immunotherapy from microcarrier cell culture, Front. Bioeng. Biotechnol. (2023), https://doi.org/10.3389/fbioe.2023.1193454.
[14] Ich, ICH Considerations: Oncolytic Viruses, 2009.
[15] for Advanced Therapies C Reflection paper on classification of advanced therapy medicinal products.
[16] I. Knezevic, G. Stacey, J. Petricciani, WHO Study Group on cell substrates for production of biologicals, Geneva, Switzerland, 11–12 June 2007, Biologicals 36 (2008) 203–211.
[17] S. Göbel, K.E. Jaén, R.P. Fernandes, M. Reiter, J. Altomonte, U. Reichl, Y. Genzel, Characterization of a quail suspension cell line for production of a fusogenic oncolytic virus, Biotechnol. Bioeng. 120 (2023) 3335–3346.
[18] J. Marek, L. Hanesch, T. Krabbe, N. El Khawanky, S. Heidegger, J. Altomonte, Oncolytic virotherapy with chimeric VSV-NDV synergistically supports RIG-I-dependent checkpoint inhibitor immunotherapy, Mol. Ther. Oncolytics 30 (2023) 117–131.
[19] S. Göbel, F. Kortum, K.J. Chavez, I. Jordan, V. Sandig, U. Reichl, J. Altomonte, Y. Genzel, Cell-line screening and process development for a fusogenic oncolytic virus in small-scale suspension cultures, Appl. Microbiol. Biotechnol. 106 (2022) 4945–4961.
[20] A. Linder, V. Bothe, N. Linder, et al., Defective Interfering Genomes and the Full-Length Viral Genome Trigger RIG-I After Infection With Vesicular Stomatitis Virus in a Replication Dependent Manner, Front. Immunol. (2021), https://doi.org/10.3389/fimmu.2021.595390.
[21] T. Li, M. Santos, A. Guttman, Ultrahigh Sensitivity Analysis of Adeno-associated Virus (AAV) Capsid Proteins by Sodium Dodecyl Sulphate Capillary Gel Electrophoresis, Chromatography Today (2020) 2–4.
[22] R.P. Fernandes, J.M. Escandell, A.C.L. Guerreiro, F. Moura, T.Q. Faria, S. B. Carvalho, R.J.S. Silva, P. Gomes-Alves, C. Peixoto, Assessing Multi-Attribute Characterization of Enveloped and Non-Enveloped Viral Particles by Capillary Electrophoresis, Viruses (2022), https://doi.org/10.3390/v14112539.
[23] M.W. Wolf, U. Reichl, Downstream processing of cell culture-derived virus particles, Expert Rev. Vaccines 10 (2011) 1451–1475.
[24] S.B. Carvalho, R. Silva, A.S. Moreira, B. Cunha, J. João, P.M. Alves, M.J. T. Carrondo, A. Xenopoulos, Efficient filtration strategies for the clarification of influenza virus-like particles derived from insect cells, Sep. Purif. Technol. (2019), https://doi.org/10.1016/j.seppur.2019.02.040.
[25] D.K. Sood, R.K. Aggarwal, S.B. Sharma, J. Sokhey, H. Singh, Study on the stability of 17D-204 yellow fever vaccine before and after stabilization.
[26] O.S. Kumru, S. Saleh-Birdjandi, L.R. Antunez, et al., Stabilization and formulation of a recombinant Human Cytomegalovirus vector for use as a candidate HIV-1 vaccine, Vaccine 37 (2019) 6696–6706.
[27] P.E. Cruz, A.C. Silva, A. Roldão, M. Carmo, M.J.T. Carrondo, P.M. Alves, Screening of novel excipients for improving the stability of retroviral and adenoviral vectors, Biotechnol. Prog. 22 (2006) 568–576.
[28] The Structure of the Fusion Glycoprotein of Newcastle Disease Virus Suggests a Novel Paradigm for the Molecular Mechanism of Membrane Fusion.
[29] K. Swanson, X. Wen, G.P. Leser, R.G. Paterson, R.A. Lamb, T.S. Jardetzky, Structure of the Newcastle disease virus F protein in the post-fusion conformation, Virology 402 (2010) 372–379.
[30] Y. Kim, D. Rana, T. Matsuura, W.J. Chung, K.C. Khulbe, Relationship between surface structure and separation performance of poly(ether sulfone) ultra-filtration membranes blended with surface modifying macromolecules, Sep. Purif. Technol. 72 (2010) 123–132.
[31] L. Besnard, V. Fabre, M. Fettig, E. Gousseinov, Y. Kawakami, N. Laroudie, C. Scanlan, P. Pattnaik, Clarification of vaccines: An overview of filter based technology trends and best practices, Biotechnol. Adv. 34 (2016) 1–13.
[32] F.M.N. Kadji, K. Kotani, H. Tsukamoto, Y. Hiraoka, K. Hagiwara, Stability of enveloped and nonenveloped viruses in hydrolyzed gelatin liquid formulation, Virol. J. (2022), https://doi.org/10.1186/s12985-022-01819-w.
[33] G. Gränicher, M. Babakhani, S. Göbel, I. Jordan, P. Marichal-Gallardo, Y. Genzel, U. Reichl, A high cell density perfusion process for Modified Vaccinia virus Ankara production: Process integration with inline DNA digestion and cost analysis, Biotechnol. Bioeng. 118 (2021) 4720–4734.
[34] Y. Shang, L. Li, T. Zhang, et al., Quantitative regulation of the thermal stability of enveloped virus vaccines by surface charge engineering to prevent the self-aggregation of attachment glycoproteins, PLoS Pathog. (2022), https://doi.org/10.1371/journal.ppat.1010564.
[35] S. Tinch, K. Szczur, W. Swaney, L. Reeves, S.R. Witting, A scalable lentiviral vector production and purification method using mustang Q chromatography and tangential flow filtration, Methods Mol. Biol. 1937 (2019) 135–153.
[36] A.S. Moreira, T.Q. Faria, J.G. Oliveira, et al., Enhancing the purification of Lentiviral vectors for clinical applications, Sep. Purif. Technol. 274 (2021) 118598.
[37] K. Kawka, A.N. Wilton, E.J. Redmond, M.F.C. Medina, B.D. Lichty, R. Ghosh, D. R. Latulippe, Comparison of the performance of anion exchange membrane materials for adenovirus purification using laterally-fed membrane chromatography, Biochem. Eng. J. 182 (2022) 108417.
[38] J.J. Labisch, G.P. Wiese, K. Pflanz, J. Linkhorst, Impact of the Membrane Structure of the Stationary Phase on Steric Exclusion Chromatography (SXC) of Lentiviral Vectors, Membranes (basel) (2023), https://doi.org/10.3390/membranes13100849.
[39] L.A. Santry, R. Jacquemart, M. Vandersluis, M. Zhao, J.M. Domm, T.M. McAusland, X. Shang, P.M. Major, J.G. Stout, S.K. Wootton, Interference chromatography: a novel approach to optimizing chromatographic selectivity and separation performance for virus purification, BMC Biotech. (2020), https://doi.org/10.1186/s12896-020-00627-w.
[40] B. Kalbfuss, M. Wolff, R. Morenweiser, U. Reichl, Purification of cell culture-derived human influenza A virus by size-exclusion and anion-exchange chromatography, Biotechnol. Bioeng. 96 (2007) 932–944.
[41] B. Zimmer, K. Summermatter, G. Zimmer, Stability and inactivation of vesicular stomatitis virus, a prototype rhabdovirus, Vet. Microbiol. 162 (2013) 78–84.
[42] S. Rani, P. Gogoi, S. Kumar, Spectrum of Newcastle disease virus stability in gradients of temperature and pH, Biologicals 42 (2014) 351–354.
[43] D. Loewe, T.A. Grein, H. Dieken, T. Weidner, D. Salzig, P. Czermak, Tangential flow filtration for the concentration of oncolytic measles virus: The influence of filter properties and the cell culture medium, Membranes (basel) (2019), https://doi.org/10.3390/membranes9120160.
[44] A. Makovitzki, E. Lerer, Y. Kafri, et al., Evaluation of a downstream process for the recovery and concentration of a Cell-Culture-Derived rVSV-Spike COVID-19 vaccine candidate, Vaccine 39 (2021) 7044–7051.
[45] S. Shoaebargh, I. Gough, M. Fe Medina, A. Smith, J. van der Heijden, B.D. Lichty, J. C. Bell, D.R. Latulippe, Sterile filtration of oncolytic viruses: An analysis of effects of membrane morphology on fouling and product recovery, J Memb Sci 548 (2018) 239–246.
[46] EMA, Guideline on Quality, non-clinical and clinical aspects of live recombinant viral vectored vaccines, Reproduction 44 (2009) 1–14.
[47] FDA, Guidance for Industry Cell Characterization and Qualification of Cell Substrates and Other Biological Materials Used in the Production of Viral Vaccines for Infectious Disease Indications, 2010, pp. 1–50.
[48] D. Loewe, H. Dieken, T.A. Grein, T. Weidner, D. Salzig, P. Czermak, Opportunities to debottleneck the downstream processing of the oncolytic measles virus, Crit. Rev. Biotechnol. 40 (2020) 247–264.
[49] M. Porosnicu, A.M. Quinson, K. Crossley, S. Luecke, U.M. Lauer, Phase i study of VSV-GP (BI 1831169) as monotherapy or combined with ezabenlimab in advanced and refractory solid tumors, Future Oncol. 18 (2022) 2627–2638.
[50] M.A. Do, A.A. Kamen, Critical assessment of purification and analytical technologies for enveloped viral vector and vaccine processing and their current limitations in resolving co-expressed extracellular vesicles, Vaccines (basel) (2021), https://doi.org/10.3390/vaccines9080823.
[51] K. Hammer, A. Kazcorowski, L. Liu, M. Behr, P. Schemmer, I. Herr, D. M. Nettelbeck, Engineered adenoviruses combine enhanced oncolysis with improved virus production by mesenchymal stromal carrier cells, Int. J. Cancer 137 (2015) 978–990.
[52] Z. Yang, B.C.M.F. Paes, J.P.C. Fulber, M.Y. Tran, O. Farnós, A.A. Kamen, Development of an Integrated Continuous Manufacturing Process for the rVSV-Vectored SARS-CoV-2 Candidate Vaccine, Vaccines (basel) (2023), https://doi.org/10.3390/vaccines11040841.
[53] S. Kiesslich, G.N. Kim, C.F. Shen, C.Y. Kang, A.A. Kamen, Bioreactor production of rVSV-based vectors in Vero cell suspension cultures, Biotechnol. Bioeng. 118 (2021) 2649–2659.
[54] D.K. Cureton, R.H. Massol, S.P.J. Whelan, T. Kirchhausen, The length of vesicular stomatitis virus particles dictates a need for actin assembly during clathrin-dependent endocytosis, PLoS Pathog. (2010), https://doi.org/10.1371/journal.ppat.1001127.
[55] A. Huang, D. Baltimore, Defective Viral Particles and Viral Disease Processes, Nature 226 (1970) 325–327.
[56] P. Von Magnus, Incomplete Forms of Influenza Virus, Adv. Virus Res. 2 (1954) 59–79.
[57] S. Göbel, K.E. Jaén, M. Dorn, V. Neumeyer, I. Jordan, V. Sandig, U. Reichl, J. Altomonte, Y. Genzel, Process intensification strategies toward cell culture-based high-yield production of a fusogenic oncolytic virus, Biotechnol. Bioeng. 120 (2023) 2639–2657.